Research Repository UCD

Title	Interferometric resolution examined by means of electromagnetic theory
Authors(s)	Körner, T. O., Sheridan, John T., Schwider, J.
Publication date	1995-04-01
Publication information	Körner, T. O., John T. Sheridan, and J. Schwider. "Interferometric Resolution Examined by Means of Electromagnetic Theory." Optical Society of America, April 1, 1995. https://doi.org/10.1364/JOSAA.12.000752.
Publisher	Optical Society of America
Item record/more information	http://hdl.handle.net/10197/3324
Publisher's statement	This paper was published in Journal of the Optical Society of America A and is made available as an electronic reprint with the permission of OSA. The paper can be found at the following URL on the OSA website: http://www.opticsinfobase.org/abstract.cfm?URI=josaa-12-4-752. Systematic or multiple reproduction or distribution to multiple locations via electronic or other means is prohibited and is subject to penalties under law.
Publisher's version (DOI)	10.1364/JOSAA.12.000752

Downloaded 2026-05-01 23:37:41

The UCD community has made this article openly available. Please share how this access benefits you. Your story matters! (@ucd_oa)

© Some rights reserved. For more information

Interferometric resolution examined by means of electromagnetic theory

T. O. Körner

Laser-Forschungslabor an der Urologischen Klinik der Ludwig-Maximilians-Universität, Marchioninistrasse 15, 81377 Munich, Germany

J. T. Sheridan and J. Schwider

Physikalisches Institut der Universität Erlangen-Nürnberg, Staudtstrasse 7/B2, 91058 Erlangen, Germany

Received August 17, 1994; revised manuscript received November 10, 1994; accepted November 10, 1994

Interferometric methods are widely used in surface metrology. A question that arises is how much information about the surface can be extracted from a given interferogram. For examination of the resolution limit of interferometry with coherent monochromatic light, interferograms of several surface relief gratings calculated with the use of approximate and rigorous theories are presented. The limits of the usefulness of scalar theory based on the use of the Fourier transform are indicated. Interferograms of dielectric and metallic structures are examined, including simple lamellar gratings and gratings made up of trapezoidal steps with varying slopes and depths. In all cases TE illumination is assumed. The effects of changing numerical aperture and defocus on the interferograms are also examined.

1. INTRODUCTION

Interferometry is a method widely used to extract metrological information about surface-relief structures.[1–7] It is popular because it is nondestructive, noninvasive, and relatively inexpensive. In general, the method is parallel; i.e., the whole object can be analyzed at once, and automatization can be achieved. It is well known that the resolution of this method is limited by the wavelength of the illuminating light and by the numerical aperture (N.A.) of the collection lens. The information extractable will also depend, however, on the type of object being tested. Within deep structures and structures with fine relief patterns multiple-scatter effects, shadowing, or strong boundary conditions may occur, leading to the generation of interferometric images that are not obviously related to the actual surface profile. Scalar transmittance theories based on the application of the Fourier transform do not take account of such effects. For modeling such cases it is necessary to apply rigorous electromagnetic theory (REMT). In this paper, to our knowledge for the first time, REMT is applied to analyze interferometric images for testing the performance that can be expected from this type of metrology.

In the field of microscopy, which is closely related to interferometry, analyses using REMT have already been carried out. Coherent and partially coherent bright-field images have been examined.[8–10] Coherent bright-field, dark-field, and confocal images of square surface-relief gratings have been examined,[11,12] and rigorous analyses of Normarski microscope images[13] have been presented. Of particular importance in metrology is the ability to identify the position of an edge. In most practical situations the edge will not be vertical but will have some slope introduced by the manufacturing process. In this paper we therefore require the use of REMT, which can deal with such slanted edge structures.

A REMT algorithm, based on the use of a piecewise description of the field inside a lamellar grating with use of Legendre polynomials,[14–18] which we refer to as the Legendre exact eigenfunction method (LM), is used to model diffraction by gratings. The LM permits the accurate calculation, for both TE- and TM-polarized incident light, of the eigenvalues of lossless and highly conducting lamellar gratings with the use of simple eigenvalue–eigenvector algorithms. With such a procedure the roots for metallic gratings are found automatically without any elaborate root-searching algorithm in the complex plane.[19,20] However, it retains the improved convergence of the exact eigenfunction method[21] in comparison with other REMT algorithms based on Fourier expansion of the grating cross-sectional permittivity.[22,23]

2. PRINCIPLES OF INTERFEROMETRIC SURFACE METROLOGY

Given an interferometric image, one has to deal with the question of how this image correlates with the surface profile of the object under examination. In general, one approaches this problem by assuming that the object can be described by a scalar transmission function,

$$t(x) = |t(x)|\exp[i\Phi(x)] \qquad \text{with } \forall x \in \mathbb{R} : \Phi(x) \in \mathbb{R}\,, \quad (1)$$

and a corresponding reflection function. It is further assumed that these functions can be obtained from simple geometrical considerations. Figure 1 shows a surface relief on a homogeneous dielectric material with a refractive index n_2 in the x interval $[x_1, x_2]$, whose profile can be described by a function $f(x)$. The coordinates were chosen to fulfill $\forall x \in [x_1, x_2] : f(x) \in [0, y_{\max}]$.

If a plane wave with amplitude U_0 and wavelength λ is incident onto the object from below in the positive y direction, the scalar-field distribution behind the dielectric

0740-3232/95/040752-09$06.00 ©1995 Optical Society of America

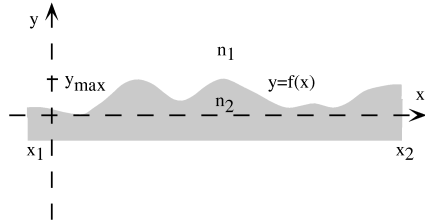

Fig. 1. Surface profile $f(x)$ on a dielectric material.

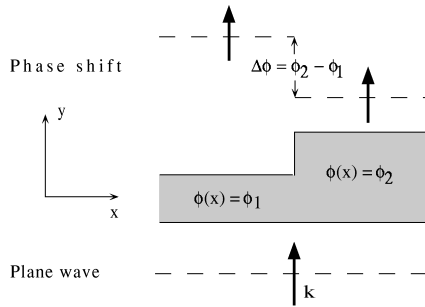

Fig. 2. Field distribution behind an edge in a dielectric grating according to Eq. (3). In the two homogeneous regions of constant thickness, $\Phi(x)$ takes on the constant values Φ_1 and Φ_2.

according to this simple model is given by

$$E(x)|_{y=y_{\max}} = U_0 t(x) \qquad \text{for } x \in [x_1, x_2]. \tag{2}$$

For the structure shown in Fig. 1, one would have $|t(x)| = 1$, $\forall x \in [x_1, x_2]$ and

$$\Phi(x) = \frac{2\pi}{\lambda} f(x)(n_2 - n_1). \tag{3}$$

An additional constant phase dilation need not to be taken into account.

Figure 2 further illustrates the above considerations for the case of a vertical edge. The z direction is perpendicular to the figure plane, and the object is assumed to be of infinite extent in this direction. Examining the structure in an interferometer with a reference wave slightly rotated about the x direction, one would obtain an interferogram as shown in Fig. 3. In the regions corresponding to constant thickness the interference fringes are straight lines. At the edge there is an abrupt displacement of the fringes. Assuming that $|t(x)| = 1$, equal intensities in the interferogram correspond to equal phase difference (modulo 2π) between the reference wave and the transmitted field. The slanted reference beam leads to a reference phase varying in the z direction. The surface profile of the structure under examination can therefore be determined from the fringe pattern obtained.[1–7]

It is known from rigorous diffraction theory[24–26] that one cannot obtain the fields behind a diffracting structure from the surface profile by using such simple considerations. The above model is an approximation that is valid only for small differences in refractive index $n_2 - n_1$, for profiles that are shallow ($y_{\max} \ll \lambda$) in comparison with the illuminating wavelength λ, and for profile functions $f(x)$ that are only slowly varying in x. For the general case, however, in order to compute the diffracted field, one has to solve Maxwell's equations, taking appropriate boundary conditions into account.

This becomes obvious if one examines interferograms of binary structures. One example of an interferogram of a lamellar grating with a period $\Lambda = 14.2\lambda$ and a thickness $h = 1.03\lambda$ (Ref. 27) is shown in Fig. 4. In the actual experiment the interferogram was obtained by use of a Mach–Zehnder interferometer with a slanted reference wave. In disagreement with Fig. 3, there is a ringing in the fringes near the edge region. Also, the fringes in regions of constant thickness are not straight but show a slightly oscillatory behavior. The simple geometrical model introduced above, which does not take diffraction effects and multiple reflection into account, therefore seems not to be sufficient for the description of the field behind a grating with such parameters.

3. INTERFEROGRAMS OF LAMELLAR DIELECTRIC GRATINGS

In order to compute the images that one would expect when examining a structure as shown in Fig. 5 with $\beta = 0°$ in an interferometer, one must first compute the electric field above or below the structure, depending on whether one is observing in transmission geometry (e.g., in a Mach–Zehnder interferometer) or in reflection geometry (e.g., in a Linnik interferometer).

Only nonevanescent waves are taken into account in the computation of the images, since only those contribute to the far field and therefore to the imaging process. For the geometry of the gratings examined in this paper,

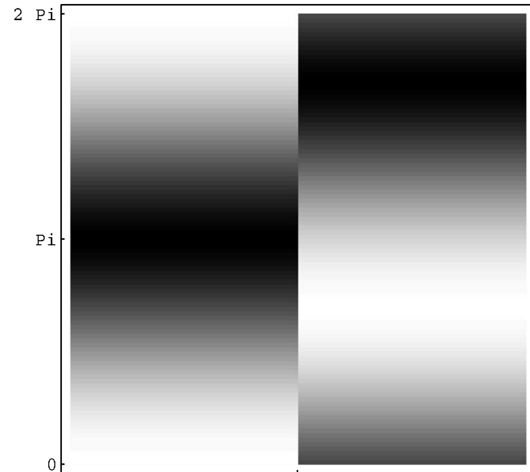

Fig. 3. Interferogram for a reference wave rotated about the x axis for a field distribution behind an edge as in Fig. 2.

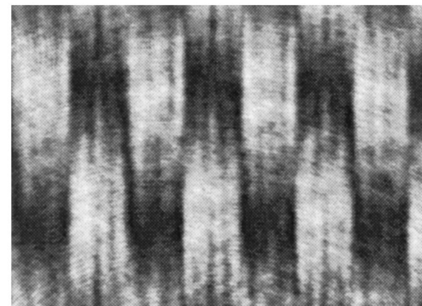

Fig. 4. Mach–Zehnder interferogram of a binary grating etched into fused silica ($n = 1.46$), $\Lambda = 9$ μm, $h = 0.656$ μm illuminated at a wavelength $\lambda = 632.8$ nm.

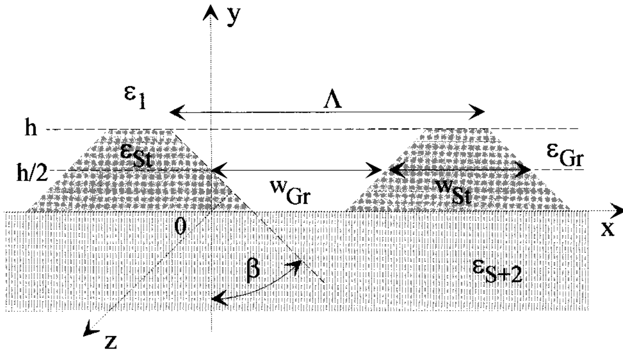

Fig. 5. Geometry and notation for a trapezoidal grating.

these fields depend on the x and y positions only and extend to infinity in the z direction. In addition, strictly monochromatic illumination is assumed. Superimposed onto the diffracted field $E(x, y)$ in the interferometer is the reference wave, which is assumed to be a plane wave incident under an angle $\phi \ll 1$ defined by

$$E^{\text{ref}}(y, z) = E_0^{\text{ref}} \exp[i(-yk_0 \cos \phi + zk_0 \sin \phi)]. \quad (4)$$

The interferograms are computed assuming perfect imaging with a magnification of 1. Therefore one obtains the intensity at x_b, z_b in the image by evaluating

$$I(x_b, z_b) = |E^{\text{ref}}(y, z) + E^d(x, y)|^2, \qquad x = x_b, z = z_b, \quad (5)$$

where the interferometer is assumed to be focused onto either the bottom $y = 0$ or the top $y = h$ of the grating illuminated from above, depending on whether one has a transmission or a reflection setup. Defocus is treated as in Refs. 11 and 12.

In this way the influences of aberrations and limitation in resolution that are due to the imaging process are not taken into account. Effects occurring in imaging with large N.A.,[28] which would require a vectorial treatment, are also left untreated. The computed images therefore show the physical limitations that exist when one is measuring surfaces by using an ideal interferometer.

The computed interferograms are presented as gray-level density plots, which is the representation most similar to the interferograms that are actually produced during measurement. This representation was preferred to contour plots, as it was found that the number of contours used could severely alter the perceived intensity information.

The first structure examined is a grating with a period $\Lambda = 10.1\lambda$; a permittivity in the step $\epsilon_{\text{St}} = 2.25$; permittivities above, below, and in the groove of $\epsilon_0 = \epsilon_2 = \epsilon_{\text{Gr}} = 1.0$; and a duty cycle of $t := w_{\text{St}}/\Lambda = 0.5$.

In a first attempt to compute the diffracted field below the grating, we used an approximate theory based on Fourier expansions (AF) of the fields incident upon the groove and the step regions. This theory was first presented as Model 3 in Ref. 29, and a corrected form was given in Ref. 27. Intrinsic to this model is the fact that the diffraction efficiencies of the even diffraction orders equal zero when the duty cycle is $t = 0.5$. Figure 6 shows the Fourier-based approximate diffracted efficiency in the third and fifth diffraction orders as a function of grating depth.

Calculations for the same structure were then carried out with the LM,[14–18] with $N = 31$ eigenfunctions retained in the computation. Figure 7 shows the efficiency in the second through fifth diffracted orders. Obviously, for thicknesses of $h > 0.6\lambda$ the even diffraction orders cannot be neglected even for this relatively large period.

The fields below the grating were computed for a thicknesses $h = 0.4\lambda$ and $h = 1.0\lambda$ for both theories, and the interferograms were synthesized. The first depth was chosen, because from Figs. 6 and 7 there is no discernible difference between the results of the two theories. The second depth, however, for this refractive index leads to the maximum displacement of the fringes in the edge region. It turned out that in this case the effects oc-

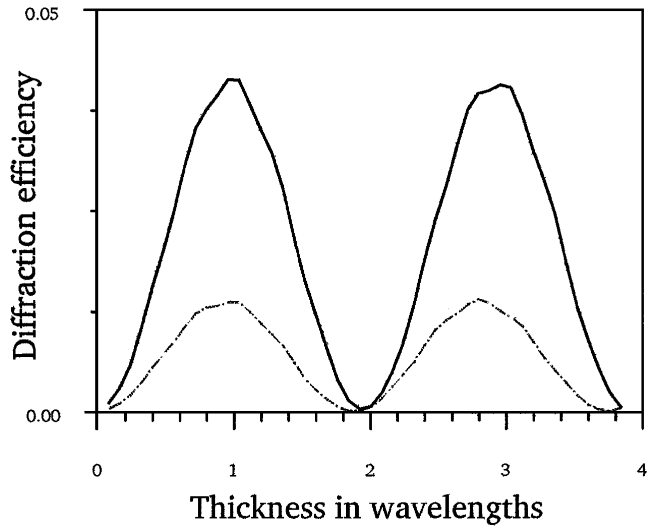

Fig. 6. Diffraction efficiencies for a lamellar grating with $\beta = 0°$, $S = 1$, $\Lambda = 10.1\lambda$, $h = 1.0\lambda$, $\epsilon_{\text{St}} = 2.25$, $\epsilon_0 = \epsilon_{\text{Gr}} = \epsilon_2 = 1.0$, and $t = 0.5$, computed with Fourier-based approximate theory. Diffraction orders: solid curve, T3; dotted–dashed curve, T5.

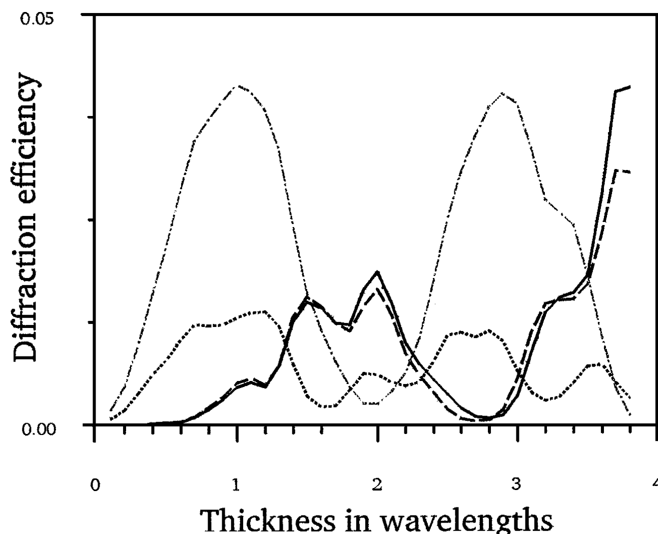

Fig. 7. As in Fig. 6 but computed by the Legendre method with number of eigenfunctions $N = 31$, maximum polynomial order in groove $m_0 = 24$, and step $m_1 = 36$. Diffraction orders: solid curve, T2; dotted–dashed curve, T3; dashed curve, T4; dotted curve, T5.

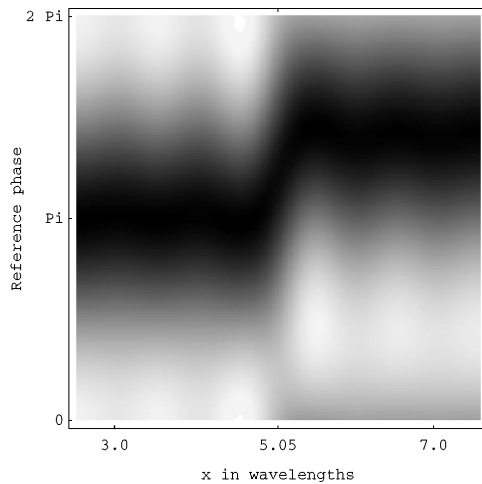

Fig. 8. Interferogram according to AF for a grating with $\Lambda = 10.1\lambda$, $\epsilon_1 = \epsilon_{\mathrm{Gr}} = \epsilon_{S+2} = 1.0$, $\epsilon_{\mathrm{St}} = 2.25$, $t = 0.5$, and $h = 0.4\lambda$; $I_{\max} = 4.86$ (with intensity incident onto the grating set to 1.0).

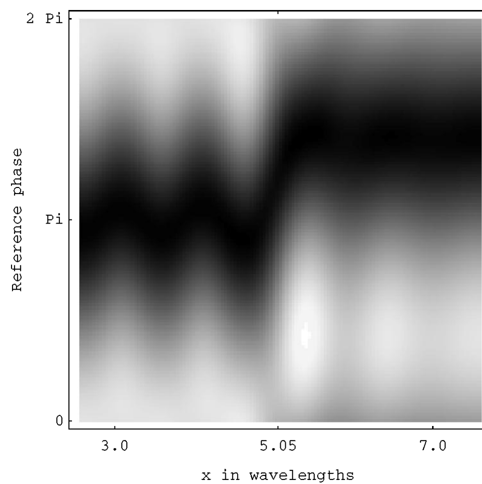

Fig. 9. As in Fig. 8 but computed according to rigorous LM with $N = 31$, $m_0 = 24$, and $m_1 = 36$; $I_{\max} = 5.51$.

curring there can be seen most distinctly. N.A. = 1 was assumed; i.e., all 21 traveling diffracted orders were retained in the synthesis of the interferogram. In all the interferograms to be presented throughout this paper the intensity of the plane wave incident onto the grating was assumed to be unity. The intensity in the reference beam was adjusted to the maximum intensity of the diffracted field in order to produce maximum visibility. Therefore the minimum intensity in all the interferograms presented is zero, corresponding to usual experimental practice. The intensities are always mapped onto the whole range of gray levels, and the maximum relative intensity (normalized with respect to the incident plane wave) $I_{\max}$ is given separately for each interferogram. Because of the symmetry of the structure and illumination with a normally incident plane wave, only half a period is shown with the reference phase between zero and 2π. The actual value of angle ϕ introduced above is therefore unimportant. The bottom of the groove is always at the left and the top of the step at the right of the interferograms.

Figures 8 and 9 show the interferograms for gratings with the above parameters according to AF and the LM, respectively. There is no distinct difference between them. Most obvious is the stronger oscillatory behavior of the fringes in the groove region when the LM is used. The thickness of the layer can be determined from the displacement of the fringes in the region about the position of the edge at $x = 5.05\lambda$. This position is marked by a small tick at the upper edge of the density plot. However, there is no abrupt displacement of fringes. The region in which the displacement takes place is $\sim 0.4\lambda$ wide. Using the simple geometric model from Section 2 for the evaluation of the interferogram, one would expect a slant angle of $\beta = 45°$. The position and the shape of the edge therefore cannot be determined exactly from the interferogram.

Next, the interferograms for a thickness $h = 1.0\lambda$ were synthesized. It can be seen from Figs. 10 and 11 that there are distinct differences between the interferograms obtained with the two different theories. It therefore seems necessary to use rigorous diffraction theory for the computation of interferograms of gratings with the above parameters.

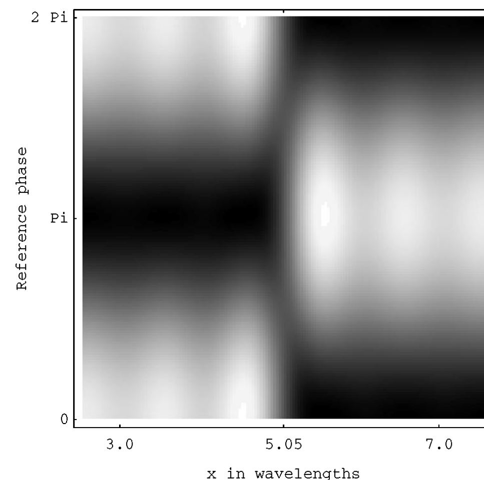

Fig. 10. Interferogram according to AF for a grating with $\Lambda = 10.1\lambda$, $\epsilon_1 = \epsilon_{\mathrm{Gr}} = \epsilon_{S+2} = 1.0$, $\epsilon_{\mathrm{St}} = 2.25$, $t = 0.5$, and $h = 1.0\lambda$; $I_{\max} = 5.5$.

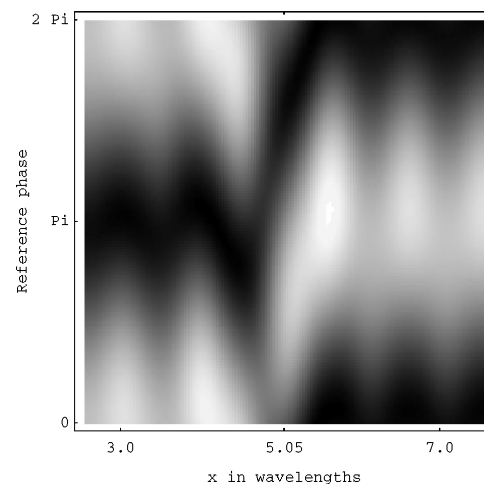

Fig. 11. As in Fig. 10 but computed according to rigorous LM with $N = 31$, $m_0 = 20$, and $m_1 = 30$; $I_{\max} = 5.51$.

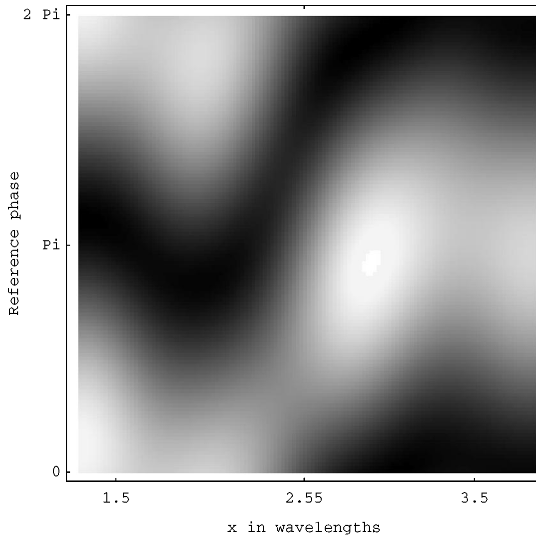

Fig. 12. Interferogram according to LM with $N = 17$, $m_0 = 10$, and $m_1 = 15$ for a grating with $\Lambda = 5.1\lambda$, $\epsilon_1 = \epsilon_{\mathrm{Gr}} = \epsilon_{S+2} = 1.0$, $\epsilon_{\mathrm{St}} = 2.25$, $t = 0.5$, and $h = 1.0\lambda$; $I_{\max} = 7.06$.

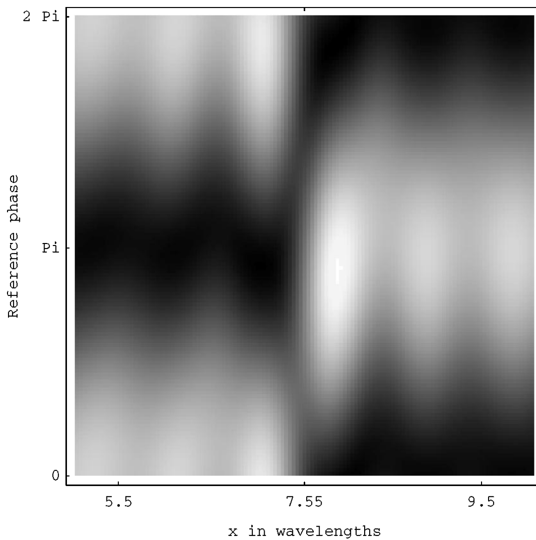

Fig. 13. Interferogram according to LM with $N = 47$, $m_0 = 30$, and $m_1 = 45$ for a grating with $\Lambda = 15.1\lambda$, $\epsilon_1 = \epsilon_{\mathrm{Gr}} = \epsilon_{S+2} = 1.0$, $\epsilon_{\mathrm{St}} = 2.25$, $t = 0.5$, and $h = 1.0\lambda$; $I_{\max} = 7.68$.

The thickness of the layer can again be determined from the displacement of the fringes at the edge. From the interferogram computed according to the LM, however, one would again expect a slanted edge ($\beta > 0$).

In order to examine the influence of structure dimensions on resolution, we computed interferograms of gratings having periods $\Lambda = 15.1\lambda$ and $\Lambda = 5.1\lambda$. Figure 12 shows an interferogram of a grating with the latter period. Again a thickness of $h = 1.0\lambda$ was chosen, with the same refractive indices as in the examples above. For such small periods it seems difficult to obtain information about the surface profile from the interferogram. The oscillatory behavior of the fringes in regions with constant thickness is so strong that even the thickness can only be estimated. The existence of a vertical edge is not at all obvious from the interferogram.

For a period $\Lambda = 15.1\lambda$, one finds the interferogram presented in Fig. 13. We show only an interval of 5.05λ about the edge at $x = 7.55\lambda$ in order to permit a better comparison with the next-smaller period examined. In this case the thickness can be well determined. The region in which the displacement of fringes takes place is narrower than 0.25λ. An estimation of the slant angle with use of the simple geometric model introduced above would yield $\beta < 14°$.

4. INTERFEROGRAMS OF STRUCTURES WITH SLANTED SLOPES

A. Dielectric Gratings in Transmission

The LM[14] as applied to lamellar gratings has been discussed in the literature for TE and TM polarization for both dielectric and metallic structures. For nonlamellar surface profiles to be dealt with, the LM has to be implemented in a way such that it can deal with gratings consisting of more than one layer.[15,16,30] One can then approximate an arbitrary surface profile by using a number of binary layers.[15] Implementation according to Suratteau[30] can be used successfully with the LM if one takes care when computing the scalar products between the eigenfunctions in the adjacent layers. This implementation, however, referred to as the T-matrix formulation,[31] might lead to numerical instabilities for thick or highly conducting gratings. Better numerical behavior is reported to be achievable with the so-called R-matrix formulation.[31] For the gratings examined in this paper, however, the T-matrix formulation turned out to be sufficient.

We examined a trapezoidal grating (see Fig. 5) with a slope angle $\beta = 45°$, a filling factor at half-height $t = 0.5$, and a thickness $h = 1.0\lambda$, with $\epsilon_0 = \epsilon_{S+2} = \epsilon_{\mathrm{Gr}} = 1.0$ and $\epsilon_{\mathrm{Gr}} = 2.25$. In an actual computation of the diffraction efficiencies for a given structure, one has to make sure that enough layers have been included to approximate

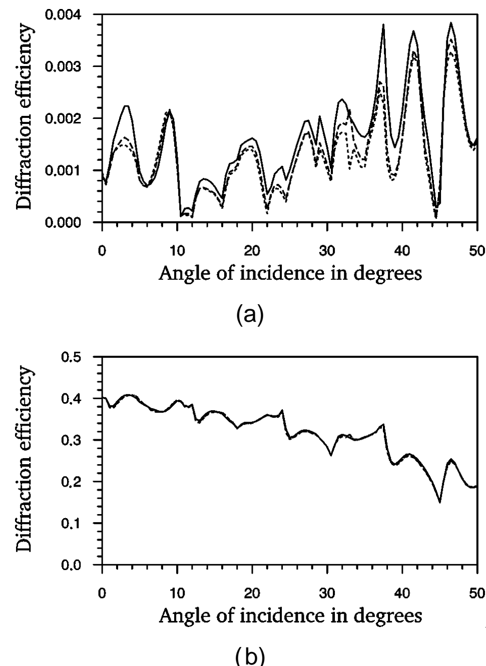

Fig. 14. Convergence of diffraction efficiency as a function of angle of incidence with varying number of layers $S \in \{4, 6, 10\}$ for the structure from Fig. 6 with $N = 37$. (a) Minus-tenth transmitted order, (b) minus-first diffracted order. Long-dashed curves, $S = 4$; solid curves, $S = 6$; dotted curves, $S = 10$.

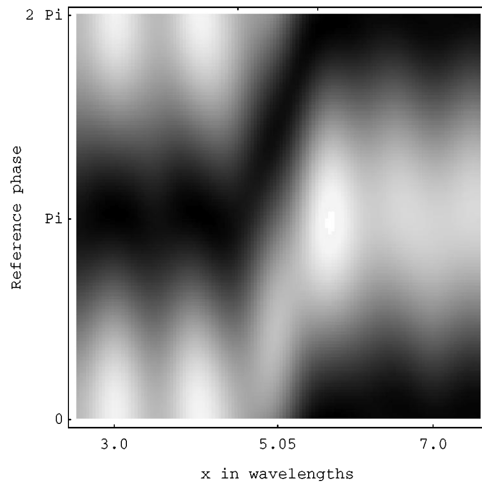

Fig. 15. Interferogram according to LM with $N = 31$, $m_0 = 24$, and $m_1 = 36$ (at half-thickness) for a trapezoidal grating with $\Lambda = 10.1\lambda$, $\beta = 45°$, $\epsilon_1 = \epsilon_{\mathrm{Gr}} = \epsilon_{S+2} = 1.0$, $\epsilon_{\mathrm{St}} = 2.25$, $t = 0.5$, and $h = 1.0\lambda$; $S = 10$, $I_{\max} = 6.45$.

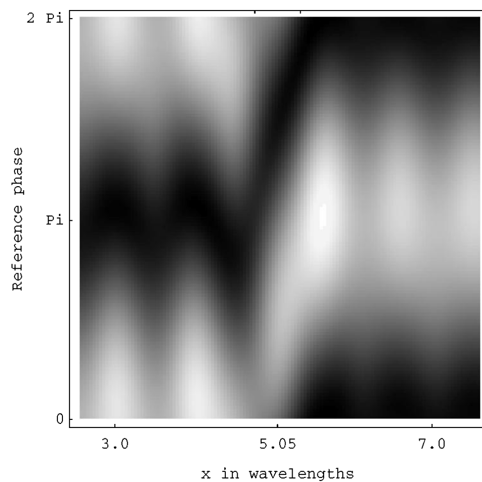

Fig. 16. Interferogram according to LM with $N = 31$, $m_0 = 24$, and $m_1 = 36$ (at half-thickness) for a trapezoidal grating with $\Lambda = 10.1\lambda$, $\beta = 30°$, $\epsilon_1 = \epsilon_{\mathrm{Gr}} = \epsilon_{S+2} = 1.0$, $\epsilon_{\mathrm{St}} = 2.25$, $t = 0.5$, and $h = 1.0\lambda$; $S = 6$ and $I_{\max} = 7.52$.

the surface of the grating. Figure 14 shows the convergence of minus-tenth and minus-first diffracted orders as a function of the angle of incidence with increasing number of layers. For the interferograms computed, only the results for perpendicular incidence are relevant. However, the angular variation curves indicate how well an arbitrary surface profile can be modeled by a multilayer structure. Whereas for the minus-first diffracted order there is no discernible difference among the cases with 4, 6, and 10 layers, for the minus-tenth diffracted order $S = 10$ layers are necessary for satisfactory convergence to be achieved.

The results that we obtained by modeling the trapezoid, using 10 layers, were then used for computing an interferogram of this structure. It was assumed that the grating was examined in a transmission setup, e.g., in a Mach–Zehnder interferometer. The interferogram can be seen in Fig. 15. The left-hand tick at the top of the density-plot frame indicates the end of the bottom of the groove, and the right-hand tick indicates the beginning of the top of the step.

In the same manner an interferogram was computed for a structure with the same period, refractive indices, and thickness but for a slope angle $\beta = 30°$. Here it turned out that for this structure the surface is sufficiently well modeled if one uses six layers in the computations. The interferogram is shown in Fig. 16. There is no discernible difference from the interferogram of the lamellar structure shown in Fig. 11; i.e., it does not seem that metrological information about this slope can be extracted from the interferogram.

Next, an interferogram for a structure with the same parameters as above but with a slope angle $\beta = 60°$ was computed. Again 10 layers were needed to ensure convergence. The result is shown in Fig. 17. It can be seen that for such a large slope angle not only can the thickness be determined from the fringe displacement, but also the slant angle can be estimated. From the width of the region in which the displacement of the fringes takes place ($\sim 1.9\lambda$), one would obtain a slant angle of $\beta \approx 62°$, using standard evaluation techniques.

From an examination of the results presented, it is clear that edges with a slope $\beta < 30°$ cannot easily be identified for a period $\Lambda = 10.1\lambda$. However, the thickness of the grating can be determined in all cases. It also became clear from further computations that for shallower gratings it is even more difficult to determine the edge angle. For a structure with $h = 0.4\lambda$, for which an interferogram for $\beta = 0°$ has already been shown in Fig. 9, it does not seem possible to resolve slant angles of $\beta < 45°$. Because of space limitations the interferograms are not presented.

Finally, an interferogram for a structure with a period of $\Lambda = 15.1\lambda$ was synthesized, as shown in Fig. 18. The slant angle was $\beta = 30°$. As can be seen, for such a big period even such a small angle can be identified from the image.

B. Metallic Structures and Linnik Reflection Interferometry

Next we computed interferograms of metallic gratings. In general, such gratings are examined in reflection, e.g.,

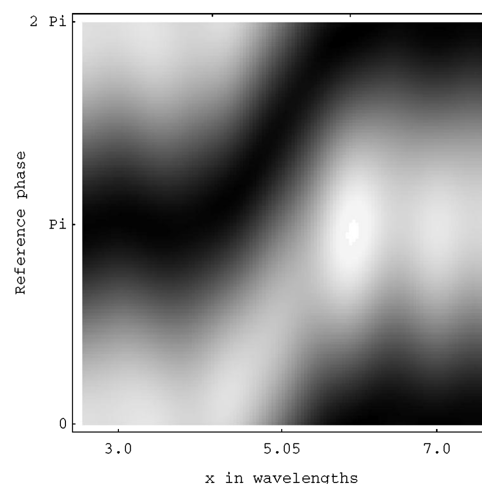

Fig. 17. Interferogram according to LM with $N = 31$, $m_0 = 24$, and $m_1 = 36$ (at half-thickness) for a trapezoidal grating with $\Lambda = 10.1\lambda$, $\beta = 60°$, $\epsilon_1 = \epsilon_{\mathrm{Gr}} = \epsilon_{S+2} = 1.0$, $\epsilon_{\mathrm{St}} = 2.25$, $t = 0.5$, and $h = 1.0\lambda$; $S = 10$ and $I_{\max} = 7.52$.

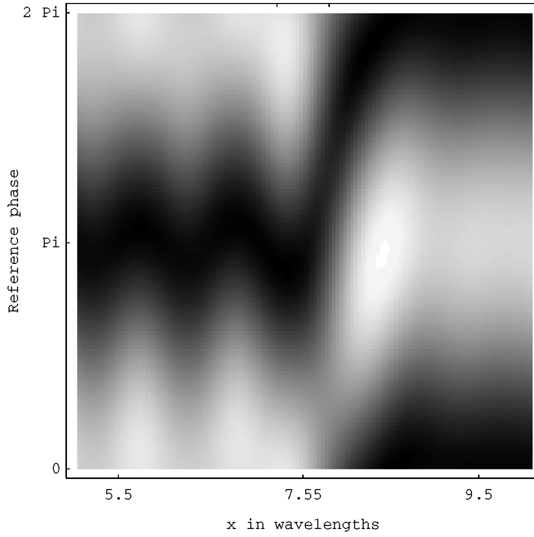

Fig. 18. Interferogram according to LM with $N = 47$, $m_0 = 30$, and $m_1 = 45$ (at half-thickness) for a trapezoidal grating with $\Lambda = 15.1\lambda$, $\beta = 30°$, $\epsilon_1 = \epsilon_{Gr} = \epsilon_{S+2} = 1.0$, $\epsilon_{St} = 2.25$, $t = 0.5$, and $h = 1.0\lambda$; $S = 6$, $I_{max} = 6.25$.

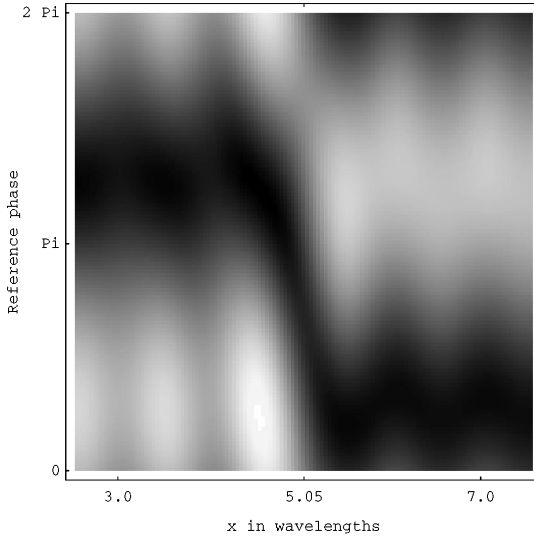

Fig. 19. Interferogram according to LM with $N = 37$, $m_0 = 20$, and $m_1 = 30$ for a binary metallic grating with $\Lambda = 10.1\lambda$, $\epsilon_1 = \epsilon_{Gr} = 1.0$, $\epsilon_{St} = \epsilon_{S+2} = -6.22 + i3.19$, $t = 0.5$, and $h = 0.25\lambda$; $I_{max} = 5.97$.

in a Linnik interferometer.[3] The complex permittivity was assumed to be $\epsilon_{S+2} = \epsilon_{St} = -6.22 + i3.19$, which is the permittivity of copper at wavelength $\lambda = 589$ nm.[1] The grating for which the computations were carried out again has a period $\Lambda = 10.1\lambda$ and a half-height duty cycle $t = 0.5$. The thickness is $h = 0.25\lambda$, which in reflection leads to a maximum displacement of interference fringes at the edge.

First, an interferogram for a lamellar structure was computed, as presented in Fig. 19. Here and in the remainder of this section it was assumed that the interferometer was focused onto the top of the grating at $y = 0.25\lambda$. Figure 20 shows the interferogram for a trapezoidal grating with a slant angle $\beta = 45°$. To ensure that enough layers were included to model the surface correctly, we computed interferograms with varying number of layers and made sure that no discernible differences occurred. As can be seen, for this angle and this period it is not possible to extract any metrological information about the exact shape of the surface. Only the thickness and the position of the edge can be estimated.

Figure 21 shows the results for a grating with a slope angle $\beta = 75°$. Here the region of the displacement of interferometric fringes is distinctly shifted with respect to the slope in the grating, which may lead to an incorrect determination of the grating duty cycle when standard evaluation techniques are applied. The same effect appeared in interferograms of trapezoidal surface profiles with smaller slope angles but was not so distinct.

C. Effects of Imaging

So far the effects of the imaging system have not been examined. We have assumed a perfect aberration-free imaging system with a magnification of 1. All high numerical aperture effects are also ignored.

To examine the effects of the imaging system, we first computed the interferogram that would be expected for the metallic structure from Fig. 19, where we assumed

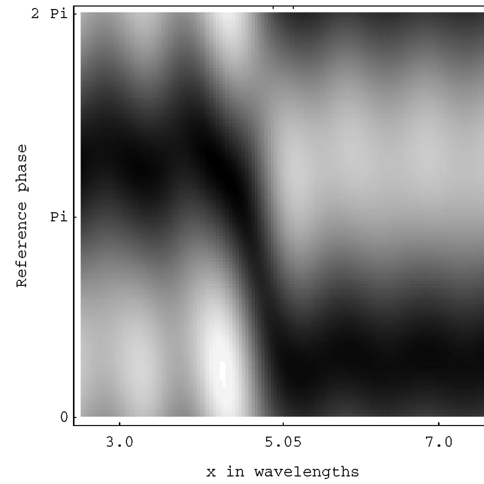

Fig. 20. Interferogram according to LM with $N = 37$, $m_0 = 20$, and $m_1 = 30$ (at half-thickness) for a trapezoidal metallic grating with $\Lambda = 10.1\lambda$, $\beta = 45°$, $\epsilon_1 = \epsilon_{Gr} = 1.0$, $\epsilon_{St} = \epsilon_{S+2} = -6.22 + i3.19$, $t = 0.5$, and $h = 0.25\lambda$; $S = 4$, $I_{max} = 5.94$.

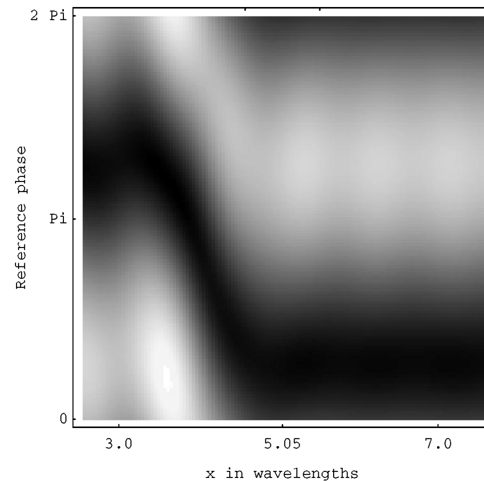

Fig. 21. Interferogram according to LM with $N = 37$, $m_0 = 20$, and $m_1 = 30$ (at half-thickness) for a trapezoidal metallic grating with $\Lambda = 10.1\lambda$, $\beta = 75°$, $\epsilon_1 = \epsilon_{Gr} = 1.0$, $\epsilon_{St} = \epsilon_{S+2} = -6.22 + i3.19$, $t = 0.5$, and $h = 0.25\lambda$; $I_{max} = 5.11$.

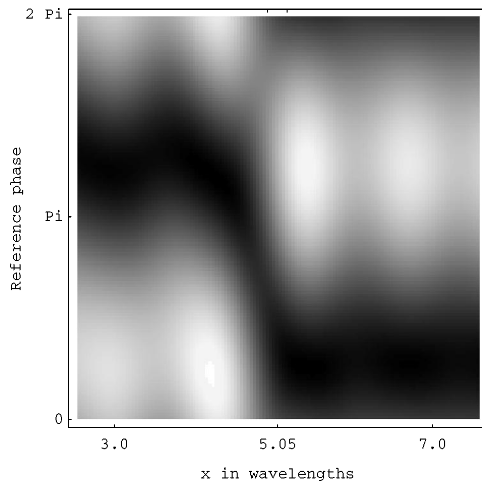

Fig. 22. Interferogram according to LM for a trapezoidal metallic grating as in Fig. 19, imaged with N.A. = 0.7, focused at the top ($y = 0.25\lambda$) of the grating, $I_{\max} = 4.6$.

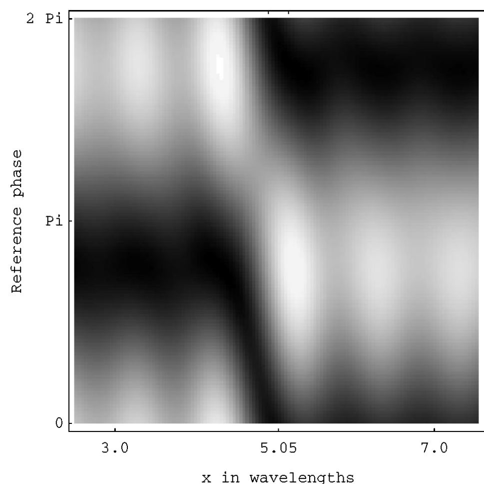

Fig. 23. Interferogram according to LM for a trapezoidal metallic grating as in Fig. 19, imaged with N.A. = 1.0, focused at the bottom of the grating at $y = 0$, $I_{\max} = 4.88$.

that the objective of the interferometer has a numerical aperture N.A. = 0.7. The number of diffraction orders retained in the formation of the image is thus reduced from 21 to 15. The result is shown in Fig. 22. From examining such images one can see that the number of oscillations in the fringes as well as the maximum intensity decreases. Therefore the region in which the displacement of the interferometric fringes takes place can be determined less exactly. This means, however, that the position and the slope of the edges are more difficult to identify as N.A. decreases.

In choosing the best focus for an interferogram the operator usually simply adjusts the focus of the objective and the reference intensity to give best contrast. For the interferograms computed for the metallic case it was assumed that the lens was focused onto the top of the grating. Practically, this is a nontrivial problem, especially when one is dealing with deep gratings with small periods, for which the focus is difficult to determine.[11] In order to make a comparison, we computed the interferogram that would be expected for the metallic grating of Fig. 19 if the objective were focused onto the bottom, $y = 0$, of the grating. We multiplied the different terms in the Rayleigh expansion[26] of the field above the grating with appropriate phase factors.[11,12] The result can be seen in Fig. 23. Defocus leads to a loss of detail and a decrease in maximum intensity.

Decreasing N.A. and defocus have similar effects on the quality of the interferogram produced. Other aberration terms can be included in this model by introduction of appropriate phase shifts in the various diffraction orders.

5. CONCLUSION

To our knowledge, REMT has been applied for the first time to the calculation of interferograms, and it has been shown that even for lamellar gratings with periods of size $\Lambda \approx 10\lambda$ and a thickness of the order of λ, scalar theory breaks down. Therefore REMT is necessary in the analysis of the interferograms of surface-relief structures with such periods and depths.

Binary and trapezoidal gratings were examined. Illumination with a monochromatic, perpendicularly impinging, TE-polarized plane wave has been assumed. The following results were found for the resolution:

Dielectric gratings ($n \approx 1.5$, i.e., fused silica at visible wavelength)

For a period $\Lambda = 10.1\lambda$

- It is possible to determine the thickness of the grating and the position of the edge.
- For a thickness $h = \lambda$, slopes with angles of $\beta \leq 30°$ cannot be distinguished from vertical edges; angles of $\beta \geq 60°$ can be estimated.
- For smaller thicknesses, less information is extractable; for $h = 0.4\lambda$, slopes having angles $\beta \leq 45°$ cannot be distinguished from vertical edges.

For a period of $\Lambda = 15.1\lambda$ a more-exact determination of the surface profile is possible; angles of $\beta = 30°$ are distinctly recognizable.

For smaller periods ($\Lambda = 5.1\lambda$), much less metrological information is extractable; even the thickness of the grating can only be estimated.

Metallic gratings (Cu at 589 nm):

For a period $\Lambda = 10.1\lambda$, a thickness $h = 0.25\lambda$, and a refractive index $\epsilon = -6.22 + i3.19$

- The thickness of the grating can be obtained from the interferogram.
- Slopes with angles $\beta < 45°$ cannot be distinguished from vertical edges.
- For greater slope angles ($45° < \beta < 75°$), standard evaluation techniques lead to errors in the determination of the edge position.

Only periodic structures with a linear slope have been examined here under TE illumination. The effects encountered with TM illumination, aberrations in the imaging system, and more-complicated surface profiles remain to be examined.

ACKNOWLEDGMENTS

J. T. Sheridan acknowledges support by the European Commission.

The authors may be contacted as follows: T. O. Körner: tel. (49) 89-7095-3722; FAX (49) 89-7095-8890; e-mail, koer@ibe.med.uni-muenchen.de; J. T. Sheridan and J. Schwider: tel. (49) 9131-858397; FAX (49) 9131-13508.

REFERENCES

1. M. Born and E. Wolf, *Principles of Optics*, 6th ed. (Pergamon, Oxford, 1980), Chap. 7.
2. M. Françon, *Optical Interferometry* (Academic, New York, 1966).
3. S. Tolansky, *An Introduction to Interferometry* (Longmans, Green, London, 1955).
4. D. Malacara, ed., *Optical Shop Testing* (Wiley, New York, 1978).
5. K. Creath, "Phase-measurement interferometry techniques," Prog. Opt. **26,** 349–393 (1988).
6. J. Schwider, "Advanced evaluation techniques in interferometry," Prog. Opt. **28,** 271–359 (1990).
7. D. W. Robinson and G. T. Reid, *Interferogram Analysis* (Institute of Physics, Bristol, UK, 1993).
8. D. Nyyssonen, "Theory of optical edge detection and imaging of thick layers," J. Opt. Soc. Am. **72,** 1425–1436 (1982).
9. D. Nyyssonen and C. P. Kirk, "Optical microscope images of thick layers with variable edge geometry: theory," J. Opt. Soc. Am. A **5,** 1270–1280 (1988).
10. J. T. Sheridan and C. J. R. Sheppard, "Micrometrology of thick structures," in *Optical Storage and Scanning Technology*, T. Wilson, ed., Proc. Soc. Photo-Opt. Instrum. Eng. **1139,** 32–39 (1989).
11. J. T. Sheridan and C. J. R. Sheppard, "Modelling of images of square-wave gratings and isolated edges using rigorous diffraction theory," Opt. Commun. **105,** 367–378 (1994).
12. J. T. Sheridan and C. J. R. Sheppard, "Coherent imaging of periodic thick fine isolated structures," J. Opt. Soc. Am. A **10,** 1–19 (1993).
13. C. M. Yuan and A. S. Strojwas, "Modeling optical microscope images of integrated-circuit structure," J. Opt. Soc. Am. A **8,** 778–790 (1991).
14. H. P. Herzig, M. T. Gale, H. W. Lehmann, and R. Morf, "Diffractive components: computer-generated elements," in *Perspectives for Parallel Optical Interconnects*, Ph. Lalanne and P. Chavel, eds., ESPRIT Basic Research Ser. 71–108 (Springer-Verlag, Berlin 1993), Chap. 5.
15. S.-E. Sandström, G. Tayeb, and R. Petit, "Lossy multistep lamellar gratings in conical diffraction mountings: an exact eigenfunction solution," J. Electromagn. Waves Appl. **7,** 631–649 (1993).
16. T. O. Körner and J. T. Sheridan, "Near fields of periodic gratings calculated using rigorous electromagnetic theory," J. Scanning **16,** 343–352 (1994).
17. J. T. Sheridan, R. Ehrhardt, and T. O. Körner, "Optimization techniques for the design of resonance domain diffractive optical elements," in *Diffractive Optics*, Vol. 11 of 1994 OSA Technical Digest Series (Optical Society of America, Washington, D.C., 1994), pp. 12–15.
18. J. T. Sheridan and T. O. Körner, "Imaging periodic surface relief structures," J. Microsc. (to be published).
19. L. C. Botten, M. S. Craig, and R. C. McPhedran, "Complex zeros of analytic functions," Comput. Phys. Commun. **29,** 245–259 (1983).
20. G. Tayeb and R. Petit, "On the numerical study of deep dielectric lamellar gratings," Opt. Acta **31,** 1361–1365 (1984).
21. L. Li and C. W. Haggans, "Convergence of the coupled-wave method for metallic lamellar diffraction gratings," J. Opt. Soc. Am. A **10,** 1184–1189 (1993).
22. K. Knop, "Rigorous diffraction theory for transmission phase gratings with deep rectangular grooves," J. Opt. Soc. Am. **68,** 1206–1210 (1978).
23. T. K. Gaylord and M. G. Moharam, "Analysis and applications of optical diffraction by gratings," Proc. IEEE **73,** 894–937 (1985).
24. R. Petit, ed., *Electromagnetic Theory of Gratings* (Springer-Verlag, Berlin, 1980).
25. D. Maystre, "Rigorous vector theories of diffraction gratings," Prog. Opt. **21,** 1–67 (1984).
26. L. C. Botten, M. S. Craig, R. C. McPhedran, J. L. Adams, and J. R. Andrewartha, "The dielectric lamellar diffraction grating," Opt. Acta **28,** 413–428 (1981).
27. M. Heissmeier, J. T. Sheridan, J. Schwider, and N. Streibl, "Detection of errors in microlithographic grating fabrication using a simple methodology," Optik **95,** 161–167 (1994).
28. B. Richards and E. Wolf, "Electromagnetic diffraction in optical systems II: structure of the image field in an aplanatic system," Proc. R. Soc. London Ser. A **253,** 358–379 (1959).
29. J. T. Sheridan and C. J. R. Sheppard, "An examination of the theories for the calculation of diffraction by square wave gratings: 3. Approximate theories," Optik **85,** 135–152 (1990).
30. J. Y. Suratteau, M. Cadilhac, and R. Petit, "Sur la détermination numérique des efficacités de certains résaux diélectriques profonds," J. Opt. (Paris) **14,** 273–288 (1983).
31. L. Li, "Multilayer modal method for diffraction gratings of arbitrary profile, depth, and permittivity," J. Opt. Soc. Am. A **10,** 2581–2591 (1993).